Scilight

Bulletin of Computational Intelligence
https://www.sciltp.com/journals/bci



Check for updates

Article

GWO-Optimized Machine Learning Models for Ultimate Bearing Capacity Prediction of Driven Piles in Cohesionless Soils

Zahra Nabavi [1,*], Athanasia D. Skentou [2,3] and Niki D. Beskou [4]

[1] Mining Engineering Department, Faculty of Engineering, Tarbiat Modares University, Tehran 14117-13116, Iran
[2] Computational Mechanics Laboratory, School of Pedagogical and Technological Education, 14121 Athens, Greece
[3] Department of Civil Engineering, University of West Attica, 12241 Athens, Greece
[4] School of Sciences and Technology, Hellenic Open University, 26335 Patras, Greece
* Correspondence: n.shaqayeq@gmail.com

How To Cite: Nabavi, Z.; Skentou, A.D.; Beskou, N.D. GWO-Optimized Machine Learning Models for Ultimate Bearing Capacity Prediction of Driven Piles in Cohesionless Soils. *Bulletin of Computational Intelligence* **2026**, *2*(4), 344–361. https://doi.org/10.53941/bci.2026.100018

Received: 13 October 2026
Revised: 31 October 2026
Accepted: 18 November 2026
Published: 25 November 2026

Abstract: Pile foundations constitute a significant fraction of building expenses, rendering the precise evaluation of ultimate bearing capacity (Q_u) essential for financial viability and structural integrity. This research examines the amalgamation of Grey Wolf Optimisation (GWO) with six machine learning methodologies: XGBoost, CatBoost, Bayesian Regularisation Neural Network (BRNN), Least Squares Support Vector Machine (LSSVM), Classification and Regression Trees (CART), and a Mamdani-type Fuzzy Inference System (FIS) as auxiliary preliminary estimation instruments in conjunction with traditional static load tests (SLT) and high-strain dynamic testing (HSDT). Employing a curated benchmark dataset comprising 59 driven pile load tests in cohesionless soils (41 for training and 18 for testing), the models integrate five geotechnical and geometric parameters: shaft friction angle (φ_s), tip friction angle (φ_t), pile length (L), cross-sectional area (A), and effective vertical stress at the pile tip ($\sigma'v$). Model efficacy is assessed using R^2, RMSE, MAE, and VAF. GWO-XGBoost attained the superior predictive precision with $R^2 = 0.9992$ (training) and $R^2 = 0.9418$ (testing), closely followed by GWO-CatBoost with $R^2 = 0.9991$ (training) and $R^2 = 0.9195$ (testing). GWO-CART and GWO-Fuzzy demonstrated somewhat elevated prediction inaccuracies, but all six GWO-optimized models effectively represented the nonlinear pile-soil interaction within the database limits. The GWO-optimized gradient boosting models serve as a quick and reliable initial screening tool within the parameter ranges of the assembled 59-case dataset, enhancing traditional geotechnical design evaluations and field load assessments.

Keywords: pile bearing capacity; Grey Wolf Optimization (GWO); XGBoost; CatBoost; machine learning; cohesionless soil; driven piles; soft computing; foundation engineering; predictive modeling

1. Introduction

The cost connected with foundation work often forms a major fraction of the total building budget [1]. As a result, the selection of an acceptable foundation structure solution and the determination of the load-bearing capability of the foundation are both key factors in the reduction of costs within building projects [2]. Because of the inherent benefits that they provide, pile foundations are not only one of the most popular deep foundation alternatives, but they are also one of the most common foundation solutions that are used today. Pile foundations are a form of foundation that are well-known for its high bearing capacity, wide range of applications, and

Copyright: © 2026 by the authors. This is an open access article under the terms and conditions of the Creative Commons Attribution (CC BY) license (https://creativecommons.org/licenses/by/4.0/).
Publisher's Note: Scilight stays neutral with regard to jurisdictional claims in published maps and institutional affiliations.

widespread usage throughout construction history. Pile construction is becoming more popular in a variety of fields, including high-rise structures, port engineering, and bridge construction, as the area of infrastructure development continues to undergo significant changes. Because it directly affects the safety and cost-effectiveness of building assignments, a pile's ultimate bearing capacities (Q_m) is essential for pile design [3]. One noteworthy aspect of the foundation for piles is its ability to shift loads into deeper soil layers [4–8]. Precise evaluation of a pile facilitates the determination of required foundation proportions and pile length, hence aiding in picking the most suitable base answer. Numerous methods, including stationary pile load testing and post-disposition analysis (PDA), could be used to perform assessment [9–11]. In addition, many standard formulas have been provided, most of which rely on the results of on-site soil analysis. Cone penetration tests (CPT) and standard penetration tests (SPT) are two examples of these formulae [12,13]. To add to this, other studies have assessed the relationship between pile movement and pile pressure using the limited element approach [14–17].

Each technique may provide various outcomes, and the dependability of the ways is affected by how accurate these predicted values are. Due to inconsistent requirements, input parameters, and oversimplifications in assumptions and relationships, analytical and experimental methods often fail to provide accurate results. Similarly, the complicated interaction between piles and soils, as well as the fluctuation of pile and soil parameters, make it difficult for numerical and regression approaches to estimate the true value of Q_m. In reality, the piles static load test (SLT) and the extreme tension dynamic weight analysis are the two basic methods for determining Q_m (HSDT) [3]. In comparison to SLT, HSDT is better since it is faster, more advanced, and cheaper. On the other hand, HSDT uses a pile driving model-based one-dimensional wave propagation analyzer (PDA), in contrast to SLT's time and cost intensity. Results from SLT and PDA tests for Q_m show excellent agreement, according to literature reviews, and standardized American techniques have helped standardize the HSDT testing process [18]. The demand for several tests in every project increases costs and time requirements, even if HSDT is quicker and cheaper than SLT. The total cost of a project may be reduced by cutting down on the number of required PDA testing. New technologies like soft computing have arisen to achieve this objective. They can anticipate Q_m more precisely than present approaches, with less tests needed and more efficient solutions to engineering difficulties [19–22]. Thus, there has been an enormous amount of focus lately on using computational methods to address geological troubles such as the Q_m [23–26]. For instance, Luo et al. [27] proposed a hybrid clever system which evaluates the Q_m in sand-based soils. More specifically, they used an improved support vector machine (SVM) powered by a genetic algorithm to create a forecasting system. Khari, Jahed Armaghani, and Harandizadeh utilized the Adaptive Neural Fuzzy Inference System (ANFIS) [28] to measure Q_u. This system took into account geometrical properties of the soil and pile, additionally SLT data and CPT data. Using the group approach to data processing and the Particle Swarm Optimization (PSO) technique, they improved the model's performance. Utilizing Genetic Programming (GP), Chen et al. [5] determined the carrying capacity of deep foundations, citing studies by Momeni et al. [4]. They claimed that the neuro-imperialism forecasting framework supplied was a reliable method for predicting Q_u. Following many soft computing techniques, Shaik et al. [29] proposed using an ANFIS algorithm for Q_m prediction. They considered input parameters such as length of pile, pile size, position of soil frictional, and vertical tension at the pile's toe. Samui [30] used support vector regression (SVR) to forecast Q_m and found that it gives a very accurate approximation of the true value. In their study, Acharyya and Dey [31], the strength of strip foundations close to a sloping ground may be determined using ANN. They generated lots of data with the finite element's software PLAXIS 2D v2015.02, with the degree of friction between the algorithm's parameters being a crucial factor overall. Nazir et al. [32] have shown that ANN is a more feasible method for forecasting the strength of bases with walls of a small thickness via Imperial Competitive Algorithms (ICA). Marto et al. [33] foster an ANN model based on PSO to evaluate the supporting strength of weak infrastructure to ANN's vulnerability to local deficits. The data collection included forty findings from thorough SLTs in coarse-grained materials as input parameters, in addition to soil contact direction, groundwater stage, and soil stress value. Pal [34] utilized pile-driven measurements obtained from 94 data sets in soil and a Generalized Regressions Neural Network (GRNN) to assess Q_m. The variables included the pushing hammer, the pushed hammer volume, the pile rise, height, underground dimension, and the pile elasticity module. Alkroosh and Nikraz [35] created an empirical formula to calculate the fundamental axial ultimate load capacity in soil cohesiveness soils using the gene expression programming (GEP) theory. This formula is beneficial for pushing bases. Maizir and Kassim [36] used ANNs to analyze 300 samples for the purpose of determining the axial capacities of the motorised piles, from worldwide civil engineering jobs in eastern Asia Kiefa [37] used the GRNN approach, accounting for the following entry variables: embedded pile size, overburden beneficial pressure, pile locale, and soil friction angle, to calculate the axial bearing capacity of driven pile in cohesive soil. Murlidhar et al. [38] used the hybrid intelligence systems GA-ANN and PSO-ANN in order to make a prediction about the Q_m. The results of their investigation demonstrated that with respect to effectiveness and fidelity to the initial procedure, the PSO-ANN forecasting

system behaved better than the GA-ANN system. Using ANN and Random Forest (RF) methods, Pham et al. [39] estimated the axial weight ability of piles. A methodology worked better than the method using ANN and other techniques for testing, In Sun et al.'s [40] analysis of Q_m, a system of recommendations with a strong correlation coefficient was created by combining the ANFIS and Firefly Algorithms (FA). Alkroosh et al. [41] outperformed typical, experimental in nature, and GEP techniques in their forecasting of the holding capacities of piles for sandy and cone soils utilizing CPT information and the results of the Least Squares Support Vectors Machine (LSSVM) method. Cantarelli et al. [42] used the ANFIS to analyze 42 data points to determine the ultimate load capacity of prefabricated concrete with reinforcement piles in Shanghai, China. By using CPT data to build an ANN-MLP model, Nejad and Jaksa [43] were able to outperform more conventional approaches to pile behaviour prediction. When compared to experimental approaches, the evolutionary polynomial regression (EPR) approach suggested by Ahangar-Asr et al. [44] for estimating piles' lateral bearing capacity was shown to be quite accurate. Bengali and Nechnech [45], Using Report Word, the system was trained with the geometric characteristics of eighty axially pressurised piles and pertinent soil information in order to examine the feasibility of employing ANN in order to predict Q_m in the sand. To predict the stationary Q_m utilizing 105 dynamic wave-stress information, Pal and Deswal [46] contrasted the outcomes of the SVM methodology to the neural network approach known as generalised regression neural network. Liu et al. [47] created a theory utilizing the SVM approach based on information acquired from 28 trials to determine the maximum load-bearing capability of piles. Yong et al. [48] created three computational techniques simulated annealing-genetics programming (GP) (SA-GP), GP tree-based, and ANFIS to ascertain the Q_m. Muduli et al. [49]. claimed to have used an extreme learning machine to forecast the side pile load capacity. According to Fatehnia and Amirinia's evaluation of smart ANN-MLP and GP strategies for measuring Q_m [50], such techniques can effectively replace analysis and empirical methodologies. In their respective studies, Jebur et al. [51] and Armaghani et al. [52] shed light on the broad use of artificial intelligence (AI) in deep foundations. These studies went beyond evaluating axial or lateral bearing capacity, including quantifying pile settling with compressive loads.

The research emphasizes the critical importance of accurately assessing the load-bearing capacity of pile foundations, a significant factor in reducing construction costs and enhancing safety in building projects. With a substantial portion of budgets allocated to foundation work, efficient evaluation methods are essential for optimizing designs. Pile foundations are favored for their high bearing capacity and versatility across various applications, making their assessment crucial for effective construction planning. It integrates machine learning algorithms, including GWO-XGBoost, GWO-CatBoost, GWO-BRNN, GWO-LSSVM, GWO-CART, and GWO-Fuzzy, to enhance predictive accuracy in estimating pile capacities. In this study, Support Vector Regression (SVR) the continuous regression formulation of the Support Vector Machine (SVM) framework (alongside its least-squares regression extension, LSSVR/LSSVM) is utilized to predict continuous ultimate bearing capacity values. The performance of these algorithms is evaluated using key metrics such as R-squared (R^2), Root Mean Square Error (RMSE), Mean Absolute Error (MAE), and Variance Accounted For (VAF). For instance, GWO-XGBoost achieved an impressive R^2 value of 0.9992 during training, indicating exceptional fit, while in testing, it retained a strong R^2 of 0.9418. These metrics illustrate the algorithms' effectiveness, with higher R^2 values reflecting better predictive performance and lower RMSE values indicating more precise estimations. Overall, the research underscores the potential of combining traditional and innovative techniques to advance foundation engineering practices, ultimately striving for improved accuracy and cost-efficiency in construction.

2. Research Methodology

2.1. Bayesian Regularization Neural Network (BRNN)

For the purpose of Bayesian regularisation training, a reverse neural network known as BRNN utilises the technique. Figuring out the number of neurons that are hidden from view is one of the difficulties that emerges throughout the process of developing a model of a neural network. The prediction performance of neural network models that are either too simple or too intricate is poorer. Both types of models have some degree of difficulty. Overfitting would occur if there were an excessive number of neurons, and this would be the opposite of what would happen if there were an inadequate number of hidden nodes. For the purpose of resolving this issue, to improve the neural network's regularization capability, the Bayesian regularization theorem is used to limit the scaling of weights and thresholds. The BRNN approach has a number of benefits, the most important of which are its capacity to identify the most effective network structures, its capacity to prevent the presence of overfitting and underearning, as well as its adequate degree of resilience [53,54].

2.2. Classification and Regression Trees (CART)

For both classification and regression trees, the CART method is responsible for their construction. The samples are divided using binary splits, and each optimum split is based on a single variable when it is performed. This approach makes use of the Gini index or towing for categorical data, and it applies techniques such as least squares for continuous variables. With a pruning method to optimize the model, CART is useful for a wide variety of data types and predictive modelling [55]. Its simplicity and binary-tree structure fit it for categorical and binary situations, making it ideal for both sorts of scenarios.

The CART method is useful because it does not rely on data type assumptions, it is able to handle complicated data, and it is flexible in that it does not pre-define rules, which makes it possible to retrieve information with ease. This makes it a perfect tool for predictive modelling across a wide range of fields since its primary strength is in the development of fully grown trees that have been optimized via pruning.

2.3. Fuzzy Inference-Based Models

With regard to fuzzy algorithms for complex systems and choices [56,57], this study also looked at the basic work that Lotfi Zadeh had done before. There was also an investigation on fuzzy inference-based models. In order to design and model solar energy systems [58] and biomedical devices [59], among other fields of usage, and due to the methodical system's robustness, accuracy, and stability, as well as the simplicity of implementation, in order to create a fuzzy inference model, we made the decision.

A fuzzy inference system (FIS) use fuzzy set theory to create a relationship between inputs (features in fuzzy classification terminology) and outputs (classes in the same terminology) [57]. This is done in order to achieve the process of mapping inputs to outputs. The Mamdani-type [60] and the Sugeno-type [61] FIS are the two fundamental kinds of fuzzy inference systems. You can get more information on these systems here. There is a consensus that both of these systems are of similar significance.

The membership functions that come out of an inference technique of the Mamdani type are really sets of fuzzy numbers. It is necessary to defuzzify each output variable when the aggregation method is finished. Each output variable is represented by a fuzzy set. A singleton output membership function is another alternative; it expresses the output as a single spike instead of a dispersed fuzzy set, which simplifies the defuzzification process. You may use the singleton membership functions. This method improves efficiency by reducing the computing complexity of finding the centroid of a two-dimensional function [61].

A comparison may be made between the Sugeno fuzzy inference technique and the Mamdani approach. The Sugeno method is comparable to the Mamdani method; however, it employs output membership functions that are either linear or constant [61]. When the Sugeno FIS is implemented, it does not make use of any output membership function, in contrast to the Mamdani method, which does employ input membership functions. Alternatively, the output is an exact number that is computed by multiplying each input by a constant and then adding up all of the results. This process is repeated until the output is obtained. Repeating this procedure until the desired result is achieved is the next step.

The Mamdani-type FIS technique [60] was used specifically for the purpose of this inquiry. First, the input variables are fuzzyfied, then fuzzy inference is performed, and finally, defuzzification is performed (Figure 1). These are the phases that make up this approach.

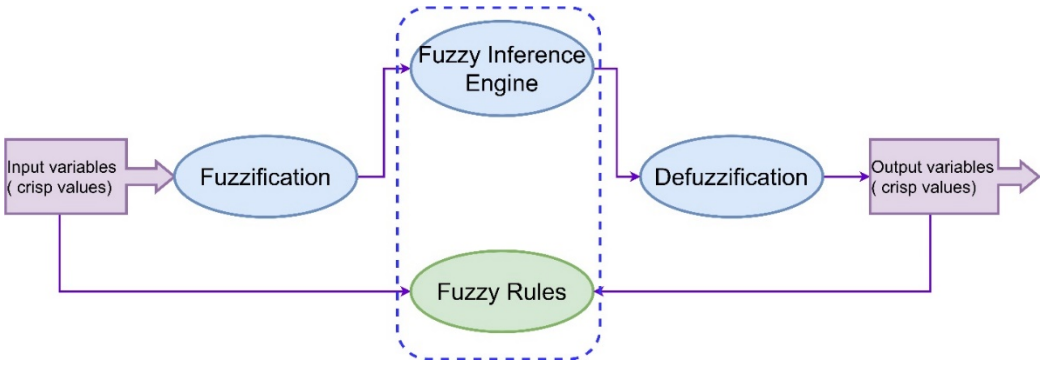

Figure 1. Fuzzy inference system.

In the first phase (fuzzification), precise geotechnical and geometric data are translated into language categories (such as low, medium, or high) by Gaussian or triangular membership functions.

In the second phase (fuzzy inference), linguistic IF–THEN rules connect the input antecedents to the output consequent by engaging and consolidating the relevant membership functions. These regulations may be derived from empirical load-test data or guided by domain mechanics; for example, if the pile embedment length (L) is classified as "long" and the tip friction angle (φ_t) is deemed "high," then the ultimate bearing capacity (Q_u) is assessed as "high.

In the final phase (defuzzification), the combined fuzzy output set is transformed into a precise numerical forecast of Q_u using conventional operators such the centroid (center of gravity), bisector, or mean of maxima.

2.4. Least Squares Support Vector Machines (LSSVM)

The LSSVM extend standard SVM by formulating regression as a system of linear Karush–Kuhn–Tucker (KKT) equations rather than a quadratic programming problem, using equality constraints and a squared-error loss function [62]. Prior to modelling, both the calibration and validation datasets underwent standardisation. After the initial configuration (with baseline regularisation $\gamma = 100$ and radial basis function kernel bandwidth $\sigma^2 = 10$), both hyperparameters underwent systematic tuning by GWO within the specified search parameters outlined in Table 1.

2.5. CatBoost

CatBoost is an open-source gradient-boosted decision tree method created by Yandex that utilises oblivious (symmetric) trees with ordered boosting to decrease prediction shift and overfitting on compact tabular datasets [63]. By using uniform splitting criteria over all nodes at an equivalent tree level, symmetric trees function as inherent structural regularizers that enhance generalisation and computing efficacy [64].

2.6. XGBoost

Extreme Gradient Boosting (XGBoost) is a scalable tree-boosting framework that sequentially constructs additive regression trees by optimizing a second-order Taylor expansion of the regularized objective function [65]. To prevent overfitting and enhance generalization, XGBoost incorporates explicit leaf-count and L2 weight penalties alongside shrinkage (learning rate) and stochastic row/column subsampling.

At each boosting iteration, XGBoost minimizes the regularized objective function defined in Equations (1) and (2):

$$\mathrm{Obj} = \sum_{i=1}^{N} L\left(\hat{y}_i, y_i\right) + \sum_{k=1}^{K} \Omega(f_k) \tag{1}$$

$$\Omega(f_k) = \gamma T + \frac{1}{2}\lambda \|w\|^2 \tag{2}$$

where L quantifies the convex loss between the measured target y_i and predicted value $\hat{y}_i$ across N training samples, f_k denotes the k-th regression tree among K total trees, w represents the vector of leaf weights, T is the number of leaves per tree, and $\Omega(f_k)$ is the regularization penalty governed by complexity parameter γ and L2 regularization coefficient λ.

2.7. GWO Algorithm

Inspired by the social hierarchy and cooperative hunting behavior of grey wolves, the Grey Wolf Optimizer (GWO) is a population-based metaheuristic algorithm [66]. The wolf pack is divided into four hierarchical levels from highest to lowest: alpha (α), beta (β), delta (δ), and omega (ω). The α wolf signifies the optimal option identified to date, while β and δ denote the second and third most effective solutions that aid in directing the pack, and ω wolves adjust their locations in relation to the three leaders. Figure 2 depicts the GWO process balancing global exploration and local exploitation.

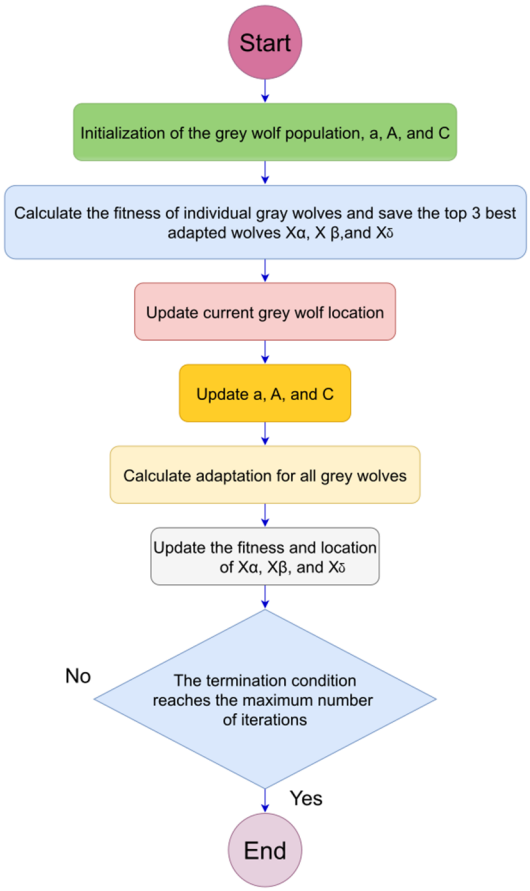

Figure 2. The flow of the Grey Wolf Optimization algorithm.

Procedure of the GWO Algorithm

1. Initialize a population of grey wolves with candidate hyperparameter vectors distributed randomly within the bounded search space, and initialize control parameters a, A, and C.
2. Evaluate the objective fitness (10-fold cross-validation RMSE on the training set) for each candidate wolf in the population.
3. Assign the top three fittest candidate solutions to the leading positions X_α (best), X_β (second best), and X_δ (third best).
4. Update the positions of all remaining candidate wolves (ω) relative to the current positions of X_α, X_β, and X_δ using the encircling and hunting equations.
5. Update the linear control parameter a and stochastic coefficient vectors A and C for the next iteration.
6. Re-evaluate the fitness of each updated grey wolf position across the population.
7. Update the leading solutions X_α, X_β, and X_δ whenever a candidate wolf achieves a lower cross-validation error.
8. Repeat Steps 4–7 until the maximum number of iterations (T_{max}) or convergence tolerance is reached, returning X_α as the optimal hyperparameter configuration.

The mathematical formulation of the GWO algorithm comprises three core phases:

2.8. Encircling Prey

During the encircling phase, grey wolves update their positions around the prey according to Equations (3) and (4):

$$D = \left| C \cdot X_p(t) - X(t) \right| \tag{3}$$

$$X(t+1) = X_p(t) - A \cdot D \tag{4}$$

where A and C are coefficient vectors, D is the distance vector between the prey and the candidate wolf, t denotes the current iteration, $X_p(t)$ is the prey position vector, and X(t) is the grey wolf position vector. The coefficient vectors A and C are computed as:

$$A = 2a \cdot r_1 - a \tag{5}$$

$$C = 2 \cdot r_2 \tag{6}$$

where r_1 and r_2 are random vectors uniformly distributed in [0, 1], and the control parameter a decreases linearly from 2 to 0 over the course of iterations ($a = 2 - 2t/T_{max}$).

2.8.1. Hunting

In an unfamiliar search domain, the actual optimum (position of the prey) is not predetermined. The GWO method posits that the three superior candidate solutions identified so far, namely the α, β, and δ wolves, provide the most dependable approximation of the optimal position. As a result, all the remaining candidate wolves (ω) adjust their placements toward the weighted locations of the α, β, and δ leaders.

Specifically, the distances to the three leading wolves and the resulting updated candidate position X(t + 1) are calculated using Equations (7)–(9):

$$\begin{aligned} D_\alpha &= |C_1 \cdot X_\alpha(t) - X(t)| \\ D_\beta &= |C_2 \cdot X_\beta(t) - X(t)| \\ D_\delta &= |C_3 \cdot X_\delta(t) - X(t)| \end{aligned} \tag{7}$$

$$\begin{aligned} X_1 &= X_\alpha(t) - A_1 \cdot D_\alpha \\ X_2 &= X_\beta(t) - A_2 \cdot D_\beta \\ X_3 &= X_\delta(t) - A_3 \cdot D_\delta \end{aligned} \tag{8}$$

$$X(t+1) = \frac{X_1 + X_2 + X_3}{3} \tag{9}$$

where D_α, D_β, and D_δ denote the distances between the α, β, and δ leaders and the candidate ω wolf, respectively, and X(t + 1) is the updated position vector.

2.8.2. Attack

Attacking the prey (exploitation) is regulated by linearly reducing a from 2 to 0 across iterations in Equation (5), which confines A to the interval [−a, a]. When |A| < 1, candidate wolves converge toward the leading solutions (local exploitation); when |A| > 1, candidate wolves diverge to explore other parts of the hyperparameter space (global exploration).

GWO Implementation and Hyperparameter Optimization

To ensure reproducibility and prevent data leakage, GWO optimization was performed exclusively within the 70% training set (N = 41) using 10-fold internal cross-validation, while the 30% hold-out testing set (N = 18) remained strictly isolated until final evaluation. The GWO population size was set to 30 search agents with a maximum of 100 iterations (stopping criterion: $T_{max} = 100$ or objective tolerance < 10^{-6}), minimizing the mean 10-fold cross-validation RMSE on the training data. Table 1 summarizes the hyperparameter search bounds and the optimal hyperparameter values identified by GWO for all six ML models.

Table 1. Hyperparameter search ranges and optimal values identified by GWO for the six ML models.

Model	Optimized Hyperparameters	Search Range	Optimal Value
GWO-BRNN	Hidden layer neurons; damping factor (μ)	Neurons: [2, 20]; μ: [10^{-4}, 10^{-1}]	Neurons = 10; μ = 0.005
GWO-CART	Max tree depth; min samples per leaf	Max depth: [2, 15]; min leaf: [1, 10]	Max depth = 6; min leaf = 2
GWO-Fuzzy	Membership functions per input; cluster radius	MFs: [2, 5]; radius: [0.1, 0.9]	MFs = 3; radius = 0.35
GWO-LSSVM	Regularization (γ); RBF kernel bandwidth (σ^2)	γ: [1, 1000]; σ^2: [0.1, 100]	γ = 145.6; σ^2 = 4.82
GWO-CatBoost	Iterations; tree depth; learning rate; L2 reg	Iter: [50, 500]; depth: [3, 8]; lr: [0.01, 0.3]; L2: [1, 10]	Iter = 300; depth = 6; lr = 0.065; L2 = 3.0
GWO-XGBoost	Estimators; max depth; learning rate; subsample	Est: [50, 500]; depth: [2, 8]; lr: [0.01, 0.3]; sub: [0.5, 1.0]	Est = 280; depth = 5; lr = 0.058; sub = 0.85

3. Data Analysis

This research assesses six machine learning algorithms optimised by GWO using a benchmark dataset of 59 static load test records for driven (displacement) piles in cohesionless soils, as prepared by Mohanty et al. [67]. The database includes a variety of sand relative densities, stress histories, geographic locations, and pile configurations. Five input parameters were identified: soil friction angle along the pile shaft (φ_s, °), soil friction angle at the pile tip (φ_t, °), pile embedment length (L, dm), pile cross-sectional area (A, dm^2), and effective vertical overburden stress at the pile tip (σ'v, MPa), with the ultimate bearing capacity (Q_u, kN) designated as the target output (Table 2). From a geotechnical standpoint, the whole axial capacity consists of shaft friction and end-bearing resistance. Shaft friction is influenced by lateral effective stress ($\sigma'h = K \cdot \sigma'v$), soil stratigraphy, and the roughness of the pile-soil interface, while the reference dataset defines the stress state through σ'v at the pile tip, in conjunction with L and φ_s, which collectively represent the physical indicators of overburden stress distribution and shaft resistance.

Table 2. Summary statistics and physical units of the driven-pile dataset (N = 59).

	N	Mean	SD	Sum	Min	Max
Q_u (kN)	59	2216.5	1246.9	130,774	75	5604
φ_s (°)	59	34.9	2.1	2057.5	28	39
φ_t (°)	59	36.4	2.1	2148	31	41
L (dm)	59	179.8	82.3	10,608	38	475
A (dm^2)	59	20.7	25.9	1218.4	3	207
σ'v (MPa)	59	0.13	0.1	7.96	0.0061	0.65

3.1. Splitting Data

The dataset was arbitrarily divided between 70% training (41 occurrences) and 30% hold-out testing (18 instances) groups before normalisation and modelling. All attributes were standardised to the range [0, 1] with parameters only derived from the training set to avert data leakage. Due to the compact nature of the combined database (N = 59, including 12 testing instances), single-split test metrics may demonstrate sensitivity to the composition of partitions; hence, 10-fold cross-validation was used inside the training set during GWO tuning to ensure consistent model selection. Figures 3 and 4 illustrate the correlation matrix and the pair panel of the variables. Significantly, Figure 4 illustrates feeble linear Pearson correlations between Q_u and both φ_s (r = 0.0456) and A (r = 0.0981), whereas σ'v (r = 0.6752), φ_t (r = 0.5186), and L (r = 0.4773) demonstrate more robust linear relationships. This illustrates the limited spectrum of φ_s (28–39°), the right-skewness in A, and the robust nonlinear interaction between pile configuration and overburden stress, which tree-based ensemble models are adept at modelling.

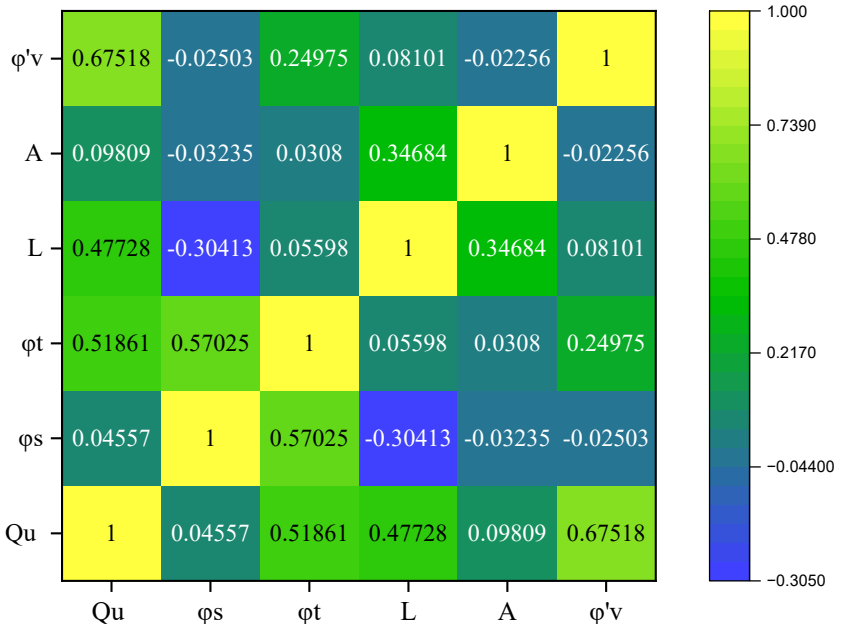

Figure 3. Correlation matrix of five input variables and one output variable.

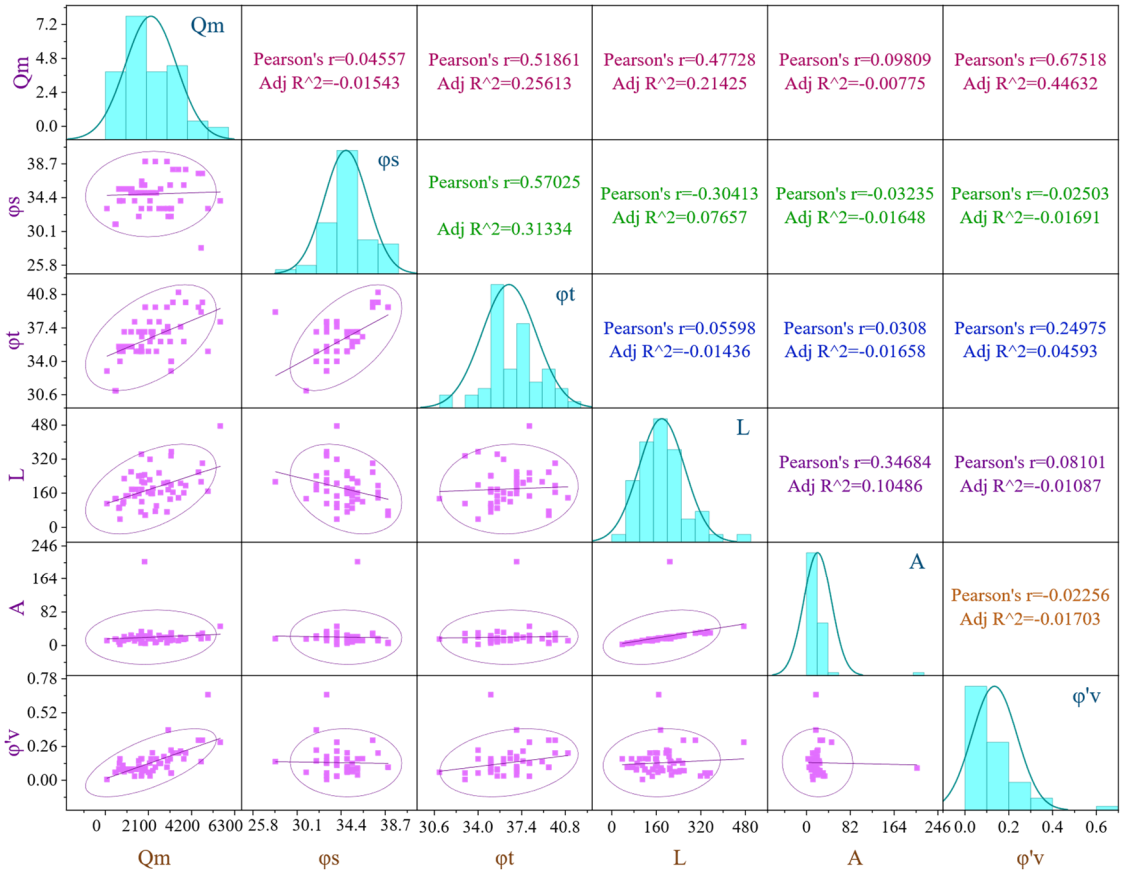

Figure 4. Pair panel of input variables.

3.2. Performance Metrics

Four statistical metrics coefficients of determination (R^2), root mean square error (RMSE), variance accounted for (VAF), and mean absolute error (MAE) were used to evaluate the predictive accuracy of the six GWO-optimized ML algorithms against measured ultimate bearing capacity values. According to Cameron and Windmeijer (1997) [68], R^2 quantifies goodness of fit as:

$$R^2 = 1 - \frac{\sum_{i=1}^{N}\left(X_i^{actual} - X_i^{predicted}\right)^2}{\sum_{i=1}^{N}\left(X_i^{actual} - \overline{X^{actual}}\right)^2} \tag{10}$$

where N represents the total number of data points, X_i^{actual} and $X_i^{predicted}$ represent the measured and predicted bearing capacity values for the i-th pile record, and $\overline{X^{actual}}$ is the mean of the measured values. The remaining error and variance metrics are defined in Equations (11)–(13):

$$RMSE = \sqrt{\frac{1}{N}\sum_{i=1}^{N}\left(X_i^{actual} - X_i^{predicted}\right)^2} \tag{11}$$

where RMSE (kN) measures the square root of the mean squared prediction error (Chai & Draxler, 2014) [69], VAF (%) quantifies the percentage of target variance explained by the model, and MAE (kN) measures the average absolute prediction error. Ideal model performance corresponds to $R^2 = 1.0$, VAF = 100%, RMSE = 0 kN, and MAE = 0 kN.

$$VAF = \left[1 - \frac{var\left(X_i^{actual} - X_i^{predicted}\right)}{var\left(X_i^{actual}\right)}\right] \times 100 \tag{12}$$

$$MAE = \frac{1}{N}\sum_{i=1}^{N}\left|X_i^{actual} - X_i^{predicted}\right| \quad (13)$$

4. Results and Comparisons

This section presents the comparative performance of the six GWO-optimized machine learning models on the training (N = 41) and hold-out testing (N = 18) datasets. All six algorithms were tuned via GWO using 10-fold cross-validation within the training set and subsequently evaluated once on the untouched testing set.

4.1. Analysis and Comparison of Six Different Machine Learning Algorithms

4.1.1. Results of the Training Dataset

In the training dataset including 41 occurrences of driven piles, the six models optimised by GWO were calibrated and assessed (Figure 5). GWO-XGBoost attained the superior training fit (R^2 = 0.9992), with GWO-CatBoost closely behind (R^2 = 0.9991). GWO-BRNN and GWO-LSSVM achieved R^2 values of 0.9358 and 0.9330, respectively, although GWO-CART (R^2 = 0.8808) and GWO-Fuzzy (R^2 = 0.8798) demonstrated somewhat worse training precision.

4.1.2. Result of the Testing Dataset

The trained models were then assessed on the 18 reserved testing examples without any adjustments (Figure 6). Upon examination of Figures 5 and 6, GWO-XGBoost exhibited the superior testing accuracy with R^2 = 0.9418, followed by GWO-CatBoost at R^2 = 0.9195. GWO-BRNN (R^2 = 0.8980), GWO-Fuzzy (R^2 = 0.8866), and GWO-CART (R^2 = 0.8724) achieved moderate testing accuracy, while GWO-LSSVM attained R^2 = 0.8607.

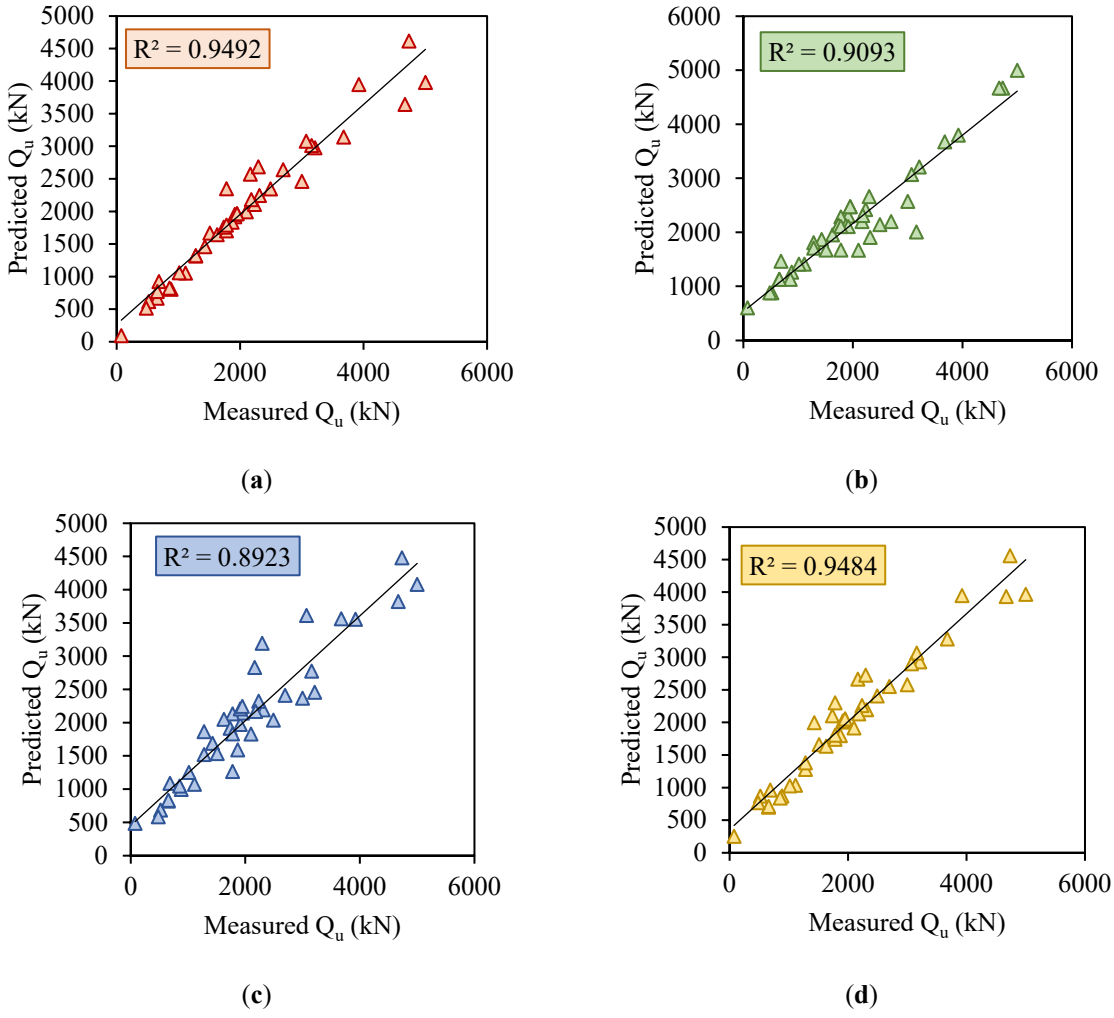

Figure 5. *Cont.*

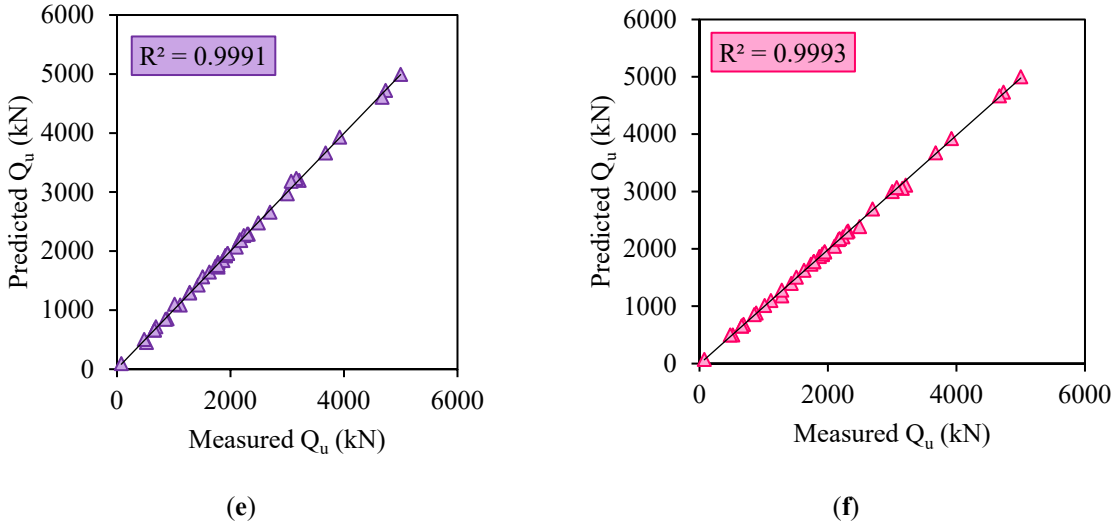

Figure 5. Regression plots for the training set of the six GWO-optimized ML algorithms: (**a**) GWO-BRNN, (**b**) GWO-CART, (**c**) GWO-Fuzzy, (**d**) GWO-LSSVM, (**e**) GWO-CatBoost, (**f**) GWO-XGBoost.

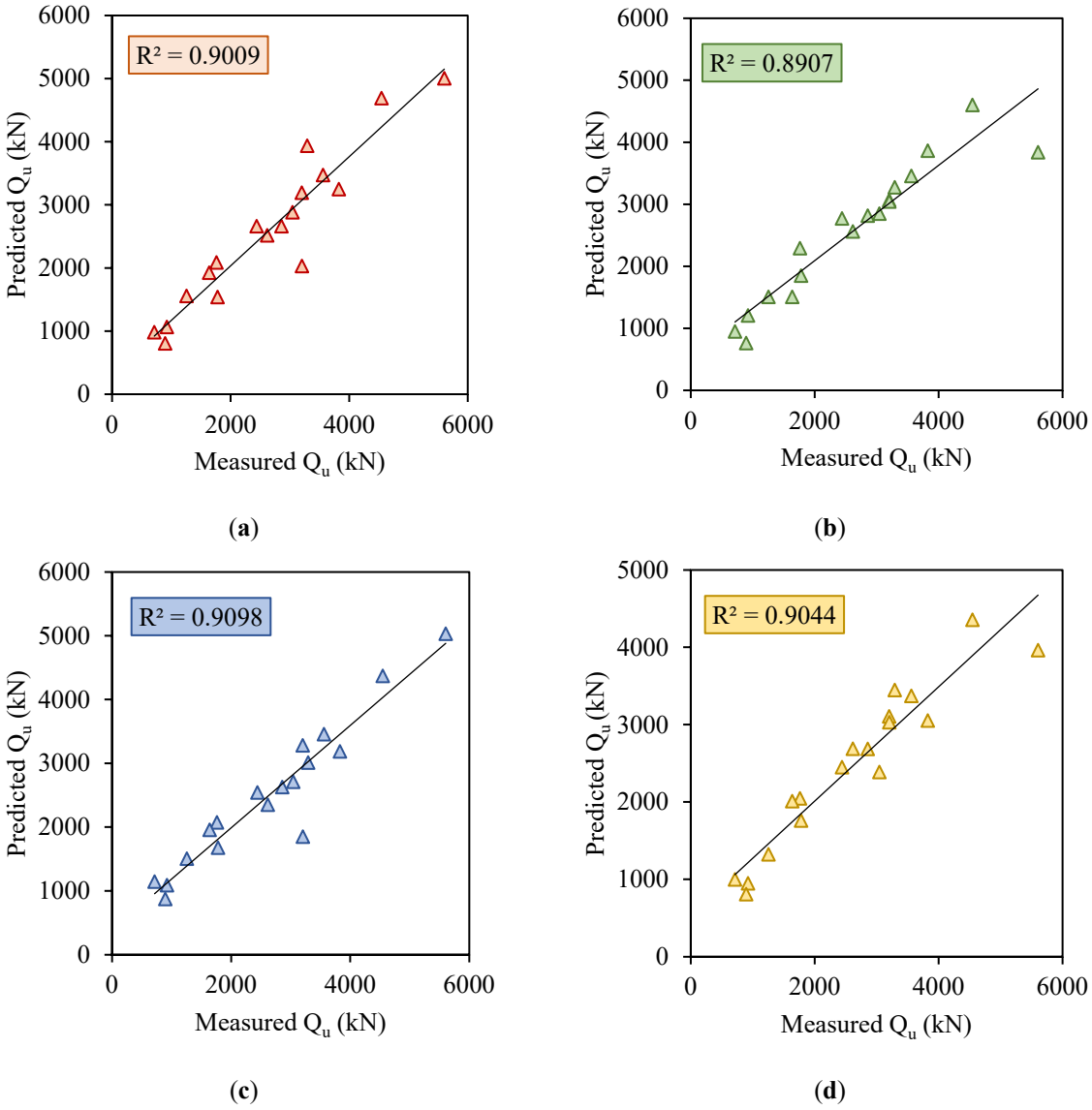

Figure 6. *Cont.*

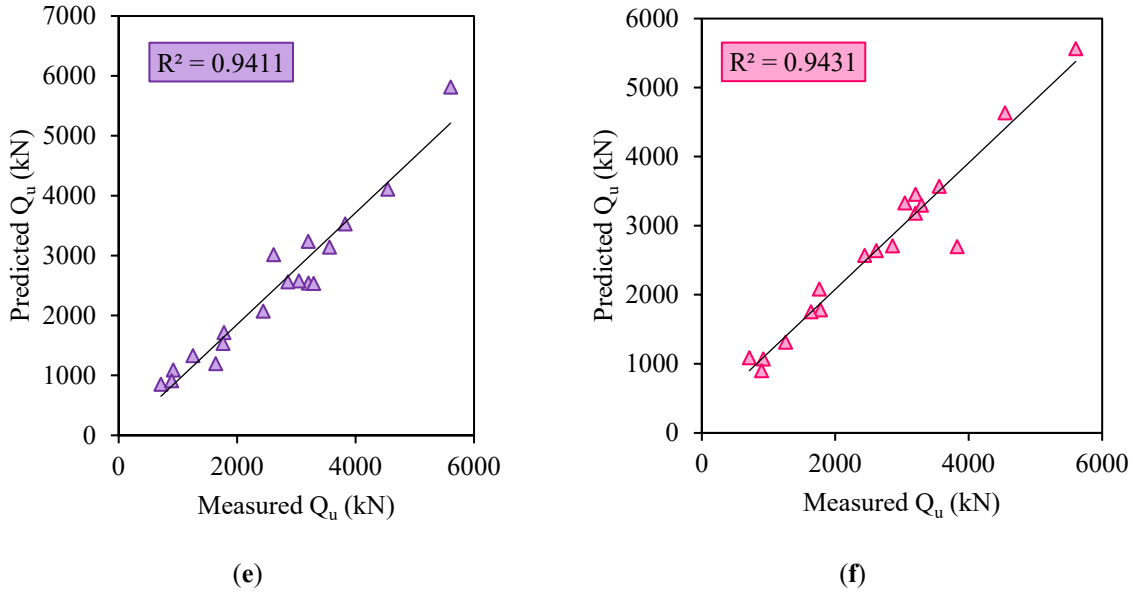

Figure 6. Regression plots for the testing set of the six GWO-optimized ML algorithms: (**a**) GWO-BRNN, (**b**) GWO-CART, (**c**) GWO-Fuzzy, (**d**) GWO-LSSVM, (**e**) GWO-CatBoost, (**f**) GWO-XGBoost.

4.1.3. Comparison of Results

Tables 3 and 4 display the quantitative assessment metrics along with their respective ordinal rank-sum scores (as per Zorlu et al., 2008 [70], allocating 6 points for the highest and 1 for the lowest per measure) during both the training and testing stages. GWO-XGBoost attained the pinnacle total score of 48 (Rank 1), exhibiting a training R^2 of 0.9993 (MAE = 14.12 kN, RMSE = 33.48 kN, VAF = 99.93%) and a testing R^2 of 0.9418 (MAE = 176.12 kN, RMSE = 312.03 kN, VAF = 94.23%). GWO-CatBoost secured the second position with an aggregate score of 38, attaining a training R^2 of 0.9991 and a testing R^2 of 0.9195 (MAE = 304.54 kN, RMSE = 366.90 kN, VAF = 94.10%).

Table 3. Evaluation metrics of the six GWO-optimized ML algorithms.

Technique	Train Phase				Test Phase			
	MAE (kN)	R^2	RMSE (kN)	VAF (%)	MAE (kN)	R^2	RMSE (kN)	VAF (%)
GWO-BRNN	164.7373	0.9358	295.8584	93.7527	309.3596	0.8980	413.1240	89.9430
GWO-CART	333.2044	0.8808	403.0586	89.9558	250.9147	0.8724	461.9854	87.3905
GWO-Fuzzy	326.2384	0.8798	404.7730	88.0161	318.3153	0.8866	435.5477	89.6998
GWO-LSSVM	205.8058	0.9330	302.1685	93.3047	292.2593	0.8607	482.6633	87.3974
GWO-CatBoost	26.3207	0.9991	35.7432	99.9066	304.5447	0.9195	366.9017	94.1030
GWO-XGBoost	14.1227	0.9992	33.4806	99.9304	176.1172	0.9418	312.0330	94.2260

Table 4. Evaluation metric ranking of the six GWO-optimized ML algorithms.

Technique	Train Phase				Test Phase				Total Rate	Rank
	MAE	R^2	RMSE	VAF	MAE	R^2	RMSE	VAF		
GWO-BRNN	4	4	4	4	2	4	4	4	30	3
GWO-CART	1	2	2	2	5	2	2	1	17	5
GWO-Fuzzy	2	1	1	1	1	3	3	3	15	6
GWO-LSSVM	3	3	3	3	4	1	1	2	20	4
GWO-CatBoost	5	5	5	5	3	5	5	5	38	2
GWO-XGBoost	6	6	6	6	6	6	6	6	48	1

The effectiveness of the six hybrid machine learning models was further evaluated using Taylor diagrams and spider (radar) charts to assess correlation, standard deviation agreement, and point-by-point tracking against measured bearing capacity.

The Taylor diagrams depicted in Figures 7 and 8 offer a concise statistical summary of the models' conformity with the observed data, employing three complementary metrics throughout both the training and testing stages: the correlation coefficient, the root-mean-square difference (RMSD), and the standard deviation. In Taylor diagrams, the reference point representing the true data is located on the *x*-axis at a correlation coefficient of 1.0. The closeness of a model's point to this benchmark signifies enhanced efficacy. The GWO-XGBoost model, shown by the orange square, is positioned closest to the reference point. It exhibits a standard deviation that closely

aligns with the observed data and a correlation coefficient that approaches 1.0. GWO-CatBoost has a minimal error rate and strong correlation, ranking as the second most effective performance, trailing closely behind. Unlike the ensemble tree-based models, GWO-CART and GWO-Fuzzy are positioned the furthest from the reference point, signifying lower correlation coefficients (below 0.95) and elevated root-mean-square errors.

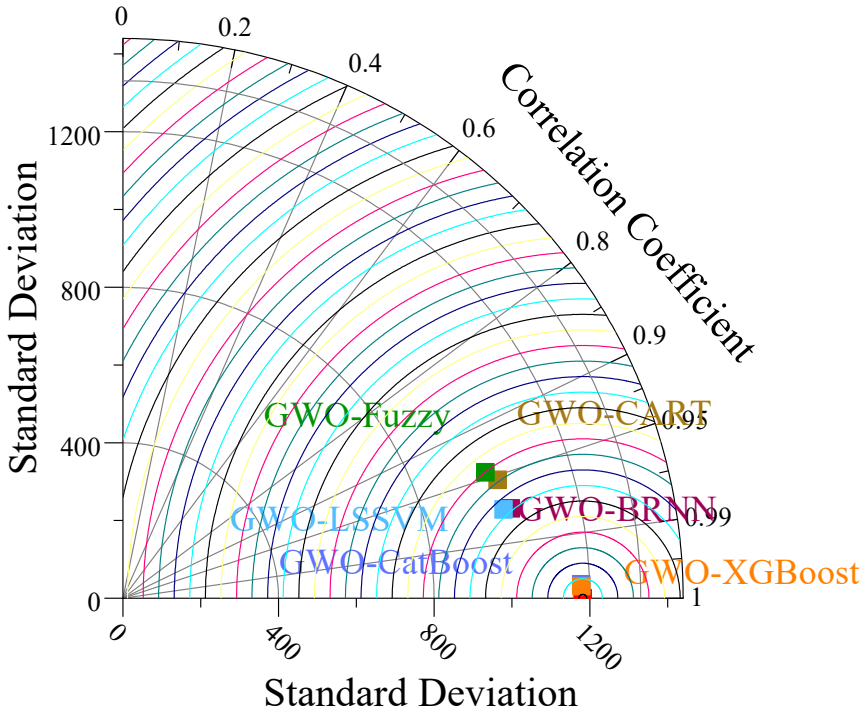

Figure 7. Taylor diagram of predicted vs. measured ultimate bearing capacity (Q_u) in the training phase.

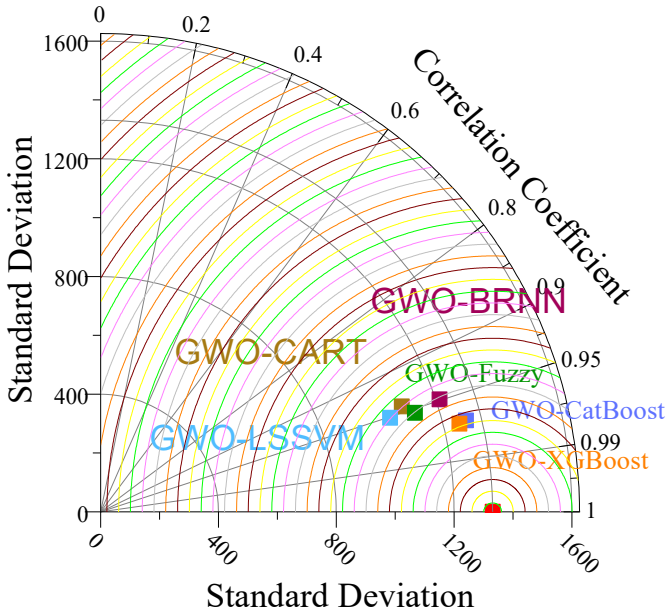

Figure 8. Taylor diagram of predicted vs. measured ultimate bearing capacity (Q_u) in the testing phase.

The radial diagrams in Figures 9 and 10 depict the relationship between the observed bearing capacity and the anticipated values at specified data indices throughout the training and testing stages. These graphs illustrate the models' ability to track fluctuations and maxima within the dataset. The GWO-XGBoost and GWO-CatBoost models consistently align with the real data points, precisely representing both the maximum and minimum limits of the bearing capacity. The GWO-CART and GWO-Fuzzy models demonstrate considerable differences, particularly at the apexes (maximum load thresholds). This suggests that although these models may capture the general trend, they struggle to accurately predict high values in the dataset, leading to the considerable mistakes shown in the statistical measures.

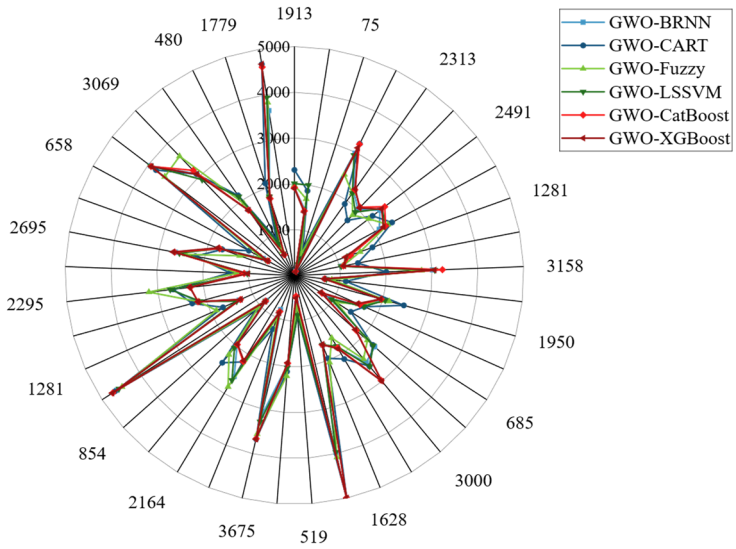

Figure 9. Comparative spider chart of predicted and measured ultimate bearing capacity (Q_u) for the training dataset.

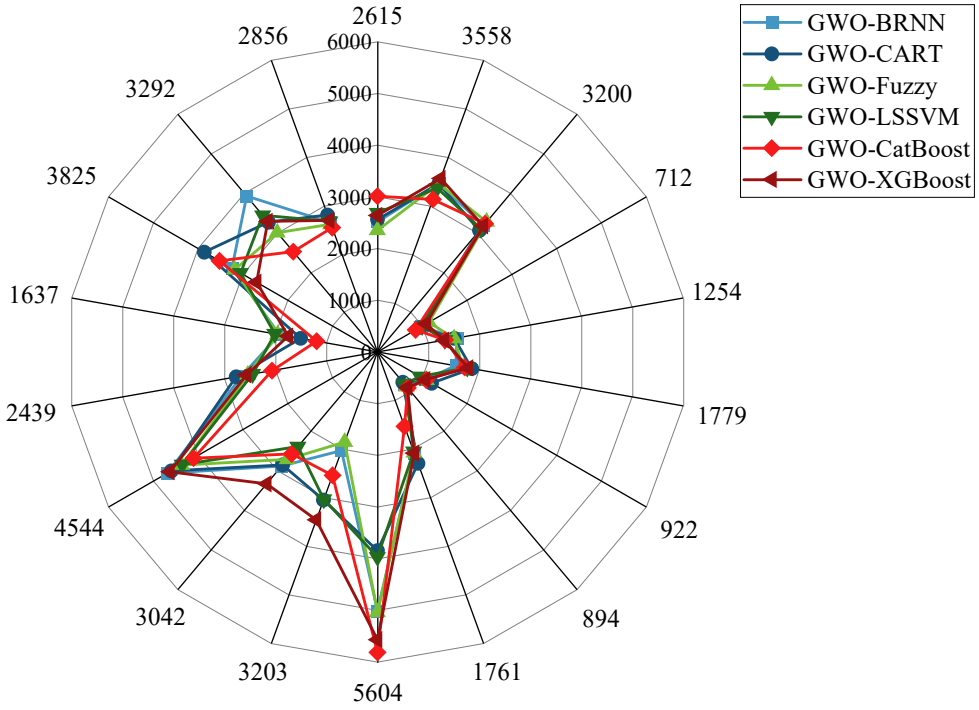

Figure 10. Comparative spider chart of predicted and measured ultimate bearing capacity (Q_u) for the testing dataset.

In aggregate, the statistical and graphical analyses suggest that GWO-XGBoost is the superior model among the six evaluated architectures on this benchmark, attaining the minimal prediction errors (Figures 7 and 8) and the most accurate monitoring of peak and trough capacity (Figures 9 and 10). From an engineering perspective, as this study centers on evaluating the six GWO-optimized architectures using the standardised 59-case Mohanty et al. [66] database, direct comparisons with unoptimised baseline models and traditional analytical/empirical methods (such as Meyerhof or CPT/SPT-based equations) were not conducted and should be a significant area for future research. Thus, the suggested models need to be used only as swift initial assessment instruments within the parameter limits outlined in Table 2, in conjunction with traditional geotechnical evaluations and site-specific load assessments.

5. Conclusions

This research assessed six machine learning algorithms enhanced by the Grey Wolf Optimiser (GWO) to forecast the ultimate bearing capacity (Q_u) of driven piles in cohesionless soils, using 59 documented load test data. Among the six hybrid models (GWO-XGBoost, GWO-CatBoost, GWO-BRNN, GWO-LSSVM, GWO-CART, and

GWO-Fuzzy), tree-based gradient boosting ensembles obtained the best accuracy. . GWO-XGBoost achieved R^2 = 0.9992 (MAE = 14.12 kN, RMSE = 33.48 kN) during training and R^2 = 0.9418 (MAE = 176.12 kN, RMSE = 312.03 kN) during testing, with GWO-CatBoost closely behind (R^2 = 0.9991 in training and R^2 = 0.9195 in testing).

The robust efficacy of GWO-XGBoost and GWO-CatBoost demonstrates their capacity to discern nonlinear relationships among the five input variables (φ_s, φ_t, L, A, and σ'v), while leveraging GWO's equilibrium between global exploration and local exploitation during the 10-fold cross-validation optimisation.

Rather of replacing static load tests (SLT) or high-strain dynamic testing (HSDT), the proposed GWO-XGBoost framework acts as a speedy, cost-effective preliminary screening tool to assist early-stage foundation design alongside standard geotechnical examinations. Numerous constraints must be acknowledged: the dataset is limited (N = 59, with 12 testing instances) and confined to driven piles in cohesionless soils, which restricts direct application to cohesive or stratified profiles. Subsequent research needs to augment the database with more field recordings, conduct formal ablation studies against unrefined baseline machine learning models and traditional analytical/empirical techniques, and integrate CPT/SPT measures together with uncertainty quantification.

Author Contributions

Z.N.: Writing—original draft preparation, conceptualization, software, methodology, validation, formal analysis, supervision; A.D.S.: Writing—review and editing, methodology, formal analysis; N.D.B.: Writing—review and editing. All authors have read and agreed to the published version of the manuscript.

Funding

This research received no external funding.

Institutional Review Board Statement

Not applicable.

Informed Consent Statement

Not applicable.

Data Availability Statement

The dataset used in this study is based on previously published data reported by Mohanty et al. [66]. The 59 driven pile load-test records used in the present analysis are available in the Appendix of the cited publication. No new experimental data were generated for this study.

Conflicts of Interest

The authors declare no conflict of interest.

Use of AI and AI-Assisted Technologies

During the preparation of this manuscript, the authors used ChatGPT (version 4) to assist with grammar, spelling, punctuation, and language refinement, as well as to improve the sentence structure and organization of some parts of the text. After using the AI tool, the authors carefully reviewed and edited the content as necessary and take full responsibility for the accuracy, originality, and integrity of the published work. The AI tool was not used to generate or interpret the research data, perform the analyses, or make scientific conclusions.

References

1. Chapman, T.; Marcetteau, A. Achieving Economy and Reliability in Piled Foundation Design for a Building Project. *Struct. Eng.* **2004**, *82*, 32–37.
2. Burland, J.B.; Broms, B.B.; de Mello, V.F.B. Behaviour of Foundations and Structures. In Proceedings of the International Conference on Soil Mechanics and Foundation Engineering, Tokyo, Japan, 10–15 July 1977; Vol. 2, pp. 495–546.
3. Kordjazi, A.; Pooya Nejad, F.; Jaksa, M.B. Prediction of ultimate axial load-carrying capacity of piles using a support vector machine based on CPT data. *Comput. Geotech.* **2014**, *55*, 91–102. https://doi.org/10.1016/j.compgeo.2013.08.001.
4. Momeni, E.; Nazir, R.; Armaghani, D.J.; et al. Prediction of pile bearing capacity using a hybrid genetic algorithm-based ANN. *Measurement* **2014**, *57*, 122–131. https://doi.org/10.1016/j.measurement.2014.08.007.

5. Chen, W.; Sarir, P.; Bui, X.N.; et al. Neuro-genetic, neuro-imperialism and genetic programing models in predicting ultimate bearing capacity of pile. *Eng. Comput.* **2020**, *36*, 1101–1115. https://doi.org/10.1007/s00366-019-00752-x.
6. Bardhan, A.; Asteris, P.G. Application of hybrid ANN paradigms built with nature inspired meta-heuristics for modelling soil compaction parameters. *Transp. Geotech.* **2023**, *41*, 100995. https://doi.org/10.1016/j.trgeo.2023.100995.
7. Khatti, J.; Kontoni, D.P.N. Assessment of Bearing Capacity of Concrete Piles in Alluvial Soils Using Bio and Swarm-Optimized Artificial Neural Network Models. *Bull. Comput. Intell.* **2025**, *1*, 53–75. https://doi.org/10.53941/bci.2025.100004.
8. Pishgahzadeh, R.; Rezakhah, M.; Batarbiat, A.; et al. A Fuzzy Multi-Criteria Decision-Making Framework for Optimal Mining Method Selection in Complex Geological Conditions. *Bull. Comput. Intell.* **2026**, *2*, 273–290. https://doi.org/10.53941/bci.2026.100015.
9. Shariatmadari, N.; Eslami, A.; Karimpour-Fard, M. Bearing Capacity of Driven Piles in Sands from SPT-Applied to 60 Case Histories. *Iran. J. Sci. Technol. Trans. B Eng.* **2008**, *32*, 125–140.
10. Zhang, C.; Nguyen, G.D.; Einav, I. The end-bearing capacity of piles penetrating into crushable soils. *Géotechnique* **2013**, *63*, 341–354. https://doi.org/10.1680/geot.11.p.117.
11. Ke, B.; Khandelwal, M.; Asteris, P.G.; et al. Rock-Burst Occurrence Prediction Based on Optimized Naïve Bayes Models. *IEEE Access* **2021**, *9*, 91347–91360. https://doi.org/10.1109/access.2021.3089205.
12. de Kuiter, J.; Beringen, F.L. Pile foundations for large North Sea structures. *Mar. Geotechnol.* **1979**, *3*, 267–314. https://doi.org/10.1080/10641197909379805.
13. Meyerhof, G.G. Bearing Capacity and Settlement of Pile Foundations. *J. Geotech. Eng. Div.* **1976**, *102*, 197–228. https://doi.org/10.1061/ajgeb6.0000243.
14. Elsherbiny, Z.H.; El Naggar, M.H. Axial compressive capacity of helical piles from field tests and numerical study. *Can. Geotech. J.* **2013**, *50*, 1191–1203. https://doi.org/10.1139/cgj-2012-0487.
15. Shooshpasha, I.; Hasanzadeh, A.; Taghavi, A. Prediction of the Axial Bearing Capacity of Piles by SPT-based and Numerical Design Methods. *Int. J. Geomate* **2013**, *4*, 560–564. https://doi.org/10.21660/2013.8.2118.
16. Thapa, I.; Ghani, S. Development of Interpretable Regression Models for Slope Stability of Nano-Silica Stabilised Soils in Mountainous Terrain. *Bull. Comput. Intell.* **2026**, *2*, 103–133. https://doi.org/10.53941/bci.2026.100006.
17. Subedi, A.; Subedi, S.; Adhikari, S.; et al. Explainable Hybridized Machine Learning for Prediction of Compressive Strength of Fly-Ash based Geopolymer Concrete. *Bull. Comput. Intell.* **2026**, *2*, 213–234. https://doi.org/10.53941/bci.2026.100012.
18. Chen, C.; Shi, L.; Shariati, M.; et al. Behavior of steel storage pallet racking connection—A review. *Steel Compos. Struct.* **2019**, *30*, 457–469. https://doi.org/10.12989/scs.2019.30.5.457.
19. Shahin, M.A.; Jaksa, M.B.; Maier, H.R. Artificial neural network applications in geotechnical engineering. *Aust. Geomech. J.* **2001**, *36*, 49–62.
20. Smola, A.J.; Schölkopf, B. A tutorial on support vector regression. *Stat. Comput.* **2004**, *14*, 199–222. https://doi.org/10.1023/b:stco.0000035301.49549.88.
21. Silewu, K.; Kahanji, C.; Simwanda, L.; et al. Intelligent Data Driven Ensemble Approaches for Bending Strength Prediction of Ultra-High Performance Concrete Beams. *Bull. Comput. Intell.* **2025**, *1*, 31–52. https://doi.org/10.53941/bci.2025.100003.
22. Iqbal, M.; Raheel, M.; Biswas, R. Hybrid Artificial Neural Network Models for Predicting Flexural Strength of FRP-Reinforced Concrete Beams. *Bull. Comput. Intell.* **2026**, *2*, 196–212. https://doi.org/10.53941/bci.2026.100011.
23. Armaghani, D.J.; Hasanipanah, M.; Amnieh, H.B.; et al. Feasibility of ICA in approximating ground vibration resulting from mine blasting. *Neural Comput. Appl.* **2018**, *29*, 457–465. https://doi.org/10.1007/s00521-016-2577-0.
24. Samui, P.; Kim, D. Least square support vector machine and multivariate adaptive regression spline for modeling lateral load capacity of piles. *Neural Comput. Appl.* **2013**, *23*, 1123–1127. https://doi.org/10.1007/s00521-012-1043-x.
25. Liao, J.; Asteris, P.G.; Cavaleri, L.; et al. Novel Fuzzy-Based Optimization Approaches for the Prediction of Ultimate Axial Load of Circular Concrete-Filled Steel Tubes. *Buildings* **2021**, *11*, 629. https://doi.org/10.3390/buildings11120629.
26. Bardhan, A.; Kardani, N. An Efficient Meta-Ensemble Paradigm for Modelling Poisson's Ratio and Maximum Horizontal Stress in Casing Collapse Hazard. *Bull. Comput. Intell.* **2026**, *2*, 146–163. https://doi.org/10.53941/bci.2026.100008.
27. Luo, Z.; Hasanipanah, M.; Amnieh, H.B.; et al. GA-SVR: A novel hybrid data-driven model to simulate vertical load capacity of driven piles. *Eng. Comput.* **2021**, *37*, 823–831. https://doi.org/10.1007/s00366-019-00858-2.
28. Harandizadeh, H.; Armaghani, D.J.; Khari, M. A new development of ANFIS–GMDH optimized by PSO to predict pile bearing capacity based on experimental datasets. *Eng. Comput.* **2021**, *37*, 685–700. https://doi.org/10.1007/s00366-019-00849-3.
29. Shaik, S.; Krishna, K.S.R.; Abbas, M.; et al. Applying several soft computing techniques for prediction of bearing capacity of driven piles. *Eng. Comput.* **2019**, *35*, 1463–1474. https://doi.org/10.1007/s00366-018-0674-7.
30. Samui, P. Prediction of pile bearing capacity using support vector machine. *Int. J. Geotech. Eng.* **2011**, *5*, 95–102. https://doi.org/10.3328/ijge.2011.05.01.95-102.

31. Acharyya, R.; Dey, A. Assessment of bearing capacity for strip footing located near sloping surface considering ANN model. *Neural Comput. Appl.* **2019**, *31*, 8087–8100. https://doi.org/10.1007/s00521-018-3661-4.
32. Nazir, R.; Momeni, E.; Marsono, K. Prediction of Bearing Capacity for Thin-Wall Spread Foundations Using Ica-Ann Predictive Model. In Proceedings of the International Conference on Civil, Structural and Transportation Engineering, Ottawa, ON, Canada, 4–5 May 2015.
33. Marto, A.; Hajihassani, M.; Momeni, E. Bearing Capacity of Shallow Foundation's Prediction through Hybrid Artificial Neural Networks. In Proceedings of the 2nd International Conference on Civil, Offshore and Environmental Engineering (ICCOEE 2014), Kuala Lumpur, Malaysia, 3–5 June 2014; pp. 681–686. https://doi.org/10.4028/www.scientific.net/amm.567.681.
34. Pal, M. Modelling Pile Capacity Using Generalised Regression Neural Network. In Proceedings of the Indian Geotechnical Conference (IGC-2011), Kochi, India, 15–17 December 2011.
35. Alkroosh, I.; Nikraz, H. Predicting axial capacity of driven piles in cohesive soils using intelligent computing. *Eng. Appl. Artif. Intell.* **2012**, *25*, 618–627. https://doi.org/10.1016/j.engappai.2011.08.009.
36. Maizir, H.; Kassim, K.A. Neural network application in prediction of axial bearing capacity of driven piles. In Proceedings of the International MultiConference of Engineers and Computer Scientists (IMECS 2013), Hong Kong, China, 13–15 March 2013; Vol. I, pp. 13–15.
37. Kiefa, M.A.A. General Regression Neural Networks for Driven Piles in Cohesionless Soils. *J. Geotech. Geoenviron. Eng.* **1998**, *124*, 1177–1185. https://doi.org/10.1061/(asce)1090-0241(1998)124:12(1177).
38. Murlidhar, B.R.; Sinha, R.K.; Mohamad, E.T.; et al. The effects of particle swarm optimisation and genetic algorithm on ANN results in predicting pile bearing capacity. *Int. J. Hydromechatron.* **2020**, *3*, 69. https://doi.org/10.1504/ijhm.2020.105484.
39. Pham, T.A.; Ly, H.B.; Tran, V.Q.; et al. Prediction of Pile Axial Bearing Capacity Using Artificial Neural Network and Random Forest. *Appl. Sci.* **2020**, *10*, 1871. https://doi.org/10.3390/app10051871.
40. Sun, G.; Hasanipanah, M.; Amnieh, H.B.; et al. Feasibility of indirect measurement of bearing capacity of driven piles based on a computational intelligence technique. *Measurement* **2020**, *156*, 107577. https://doi.org/10.1016/j.measurement.2020.107577.
41. Alkroosh, I.S.; Bahadori, M.; Nikraz, H.; et al. Regressive approach for predicting bearing capacity of bored piles from cone penetration test data. *J. Rock Mech. Geotech. Eng.* **2015**, *7*, 584–592. https://doi.org/10.1016/j.jrmge.2015.06.011.
42. Cantarelli, C.C.; Flybjerg, B.; Molin, E.J.E.; et al. Cost Overruns in Large-Scale Transport Infrastructure Projects: Explanations and Their Theoretical Embeddedness. *Eur. J. Transp. Infrastruct. Res.* **2010**, *10*, 5–18.
43. Pooya Nejad, F.; Jaksa, M.B. Load-settlement behavior modeling of single piles using artificial neural networks and CPT data. *Comput. Geotech.* **2017**, *89*, 9–21. https://doi.org/10.1016/j.compgeo.2017.04.003.
44. Ahangar-Asr, A.; Javadi, A.A.; Johari, A.; et al. Lateral load bearing capacity modelling of piles in cohesive soils in undrained conditions: An intelligent evolutionary approach. *Appl. Soft Comput.* **2014**, *24*, 822–828. https://doi.org/10.1016/j.asoc.2014.07.027.
45. Benali, A.; Nechnech, A. Prediction of the Pile Capacity in Purely Coherent Soils Using the Approach of the Artificial Neural Networks. In Proceedings of the 2nd International Seminar on Innovation and Valorization in Civil Engineering and Construction Materials (INVACO2 2011), Rabat, Morocco, 23–25 November 2011.
46. Pal, M.; Deswal, S. Modeling Pile Capacity Using Support Vector Machines and Generalized Regression Neural Network. *J. Geotech. Geoenviron. Eng.* **2008**, *134*, 1021–1024. https://doi.org/10.1061/(asce)1090-0241(2008)134:7(1021).
47. Liu, Y.J.; Liang, S.H.; Wu, J.W.; et al. Prediction Method of Vertical Ultimate Bearing Capacity of Single Pile Based on Support Vector Machine. *Adv. Mater. Res.* **2011**, *168–170*, 2278–2282. https://doi.org/10.4028/www.scientific.net/AMR.168-170.2278.
48. Yong, W.; Zhou, J.; Armaghani, D.J.; et al. A new hybrid simulated annealing-based genetic programming technique to predict the ultimate bearing capacity of piles. *Eng. Comput.* **2020**, *37*, 2111–2127. https://doi.org/10.1007/s00366-019-00932-9.
49. Muduli, P.K.; Das, S.K.; Das, M.R. Prediction of lateral load capacity of piles using extreme learning machine. *Int. J. Geotech. Eng.* **2013**, *7*, 388–394. https://doi.org/10.1179/1938636213z.00000000041.
50. Fatehnia, M.; Amirinia, G. A review of Genetic Programming and Artificial Neural Network applications in pile foundations. *Int. J. Geo-Eng.* **2018**, *9*, 2. https://doi.org/10.1186/s40703-017-0067-6.
51. Jebur, A.A.; Atherton, W.; Al Khaddar, R.M.; et al. Artificial neural network (ANN) approach for modelling of pile settlement of open-ended steel piles subjected to compression load. *Eur. J. Environ. Civ. Eng.* **2021**, *25*, 429–451. https://doi.org/10.1080/19648189.2018.1531269.
52. Armaghani, D.J.; Asteris, P.G.; Fatemi, S.A.; et al. On the Use of Neuro-Swarm System to Forecast the Pile Settlement. *Appl. Sci.* **2020**, *10*, 1904. https://doi.org/10.3390/app10061904.
53. Glória, L.S.; Cruz, C.D.; Vieira, R.A.M.; et al. Accessing marker effects and heritability estimates from genome prediction by Bayesian regularized neural networks. *Livest. Sci.* **2016**, *191*, 91–96. https://doi.org/10.1016/j.livsci.2016.07.015.

54. Tien Bui, D.; Pradhan, B.; Lofman, O.; et al. Landslide susceptibility assessment in the Hoa Binh province of Vietnam: A comparison of the Levenberg–Marquardt and Bayesian regularized neural networks. *Geomorphology* **2012**, *171–172*, 12–29. https://doi.org/10.1016/j.geomorph.2012.04.023.
55. Sutton, C.D. Classification and Regression Trees, Bagging, and Boosting. In *Handbook of Statistics 24: Data Mining and Data Visualization*; Elsevier: Amsterdam, The Netherlands, 2005; Vol. 24, pp. 303–329. https://doi.org/10.1016/s0169-7161(04)24011-1.
56. Guillaume, S. Designing fuzzy inference systems from data: An interpretability-oriented review. *IEEE Trans. Fuzzy Syst.* **2001**, *9*, 426–443. https://doi.org/10.1109/91.928739.
57. Zadeh, L.A.; Klir, G.J.; Yuan, B. *Fuzzy Sets, Fuzzy Logic, and Fuzzy Systems: Selected Papers*; World Scientific: Singapore, 1996. https://doi.org/10.1142/2895.
58. Kalogirou, S.A. *Solar Energy Engineering: Processes and Systems*, 3rd ed.; Elsevier: London, UK, 2023.
59. Velázquez, D.R.T.; Louzada, D.R.; Monteiro, E.C.; et al. Multi-parameter fuzzy design space for QbD approach applied in the development of biomedical devices. *J. Phys. Conf. Ser.* **2018**, *1044*, 012051. https://doi.org/10.1088/1742-6596/1044/1/012051.
60. Mamdani, E.H.; Assilian, S. An experiment in linguistic synthesis with a fuzzy logic controller. *Int. J. Man-Mach. Stud.* **1975**, *7*, 1–13. https://doi.org/10.1016/s0020-7373(75)80002-2.
61. Sugeno, M. *Industrial Applications of Fuzzy Control*; Elsevier Science Inc.: New York, NY, USA, 1985.
62. de Kruif, B.J.; de Vries, T.J.A. Pruning error minimization in least squares support vector machines. *IEEE Trans. Neural Netw.* **2003**, *14*, 696–702. https://doi.org/10.1109/tnn.2003.810597.
63. Hancock, J.T.; Khoshgoftaar, T.M. CatBoost for big data: An interdisciplinary review. *J. Big Data* **2020**, *7*, 94. https://doi.org/10.1186/s40537-020-00369-8.
64. Huang, G.; Wu, L.; Ma, X.; et al. Evaluation of CatBoost method for prediction of reference evapotranspiration in humid regions. *J. Hydrol.* **2019**, *574*, 1029–1041. https://doi.org/10.1016/j.jhydrol.2019.04.085.
65. Chen, T.; Guestrin, C. XGBoost: A Scalable Tree Boosting System. In Proceedings of the KDD'16: The 22nd ACM SIGKDD International Conference on Knowledge Discovery and Data Mining, San Francisco, CA, USA, 13–17 August 2016; pp. 785–794. https://doi.org/10.1145/2939672.2939785.
66. Mirjalili, S.; Mirjalili, S.M.; Lewis, A. Grey Wolf Optimizer. *Adv. Eng. Softw.* **2014**, *69*, 46–61. https://doi.org/10.1016/j.advengsoft.2013.12.007.
67. Mohanty, R.; Suman, S.; Das, S.K. Prediction of vertical pile capacity of driven pile in cohesionless soil using artificial intelligence techniques. *Int. J. Geotech. Eng.* **2018**, *12*, 209–216. https://doi.org/10.1080/19386362.2016.1269043.
68. Cameron, A.C.; Windmeijer, F.A.G. An R-squared measure of goodness of fit for some common nonlinear regression models. *J. Econom.* **1997**, *77*, 329–342. https://doi.org/10.1016/S0304-4076(96)01818-0.
69. Chai, T.; Draxler, R.R. Root mean square error (RMSE) or mean absolute error (MAE)?—Arguments against avoiding RMSE in the literature. *Geosci. Model Dev.* **2014**, *7*, 1247–1250. https://doi.org/10.5194/gmd-7-1247-2014.
70. Zorlu, K.; Gokceoglu, C.; Ocakoglu, F.; et al. Prediction of uniaxial compressive strength of sandstones using petrography-based models. *Eng. Geol.* **2008**, *96*, 141–158. https://doi.org/10.1016/j.enggeo.2007.10.009.